Environmental Science and Pollution Research (2019) 26:27940–27952
https://doi.org/10.1007/s11356-019-05976-4

RESEARCH ARTICLE

Fe-modified Ce-MnO_x/ACF_N catalysts for selective catalytic reduction of NO_x by NH_3 at low-middle temperature

Tian Gu[1] · Fengyu Gao[1,2] · Xiaolong Tang[1,2] · Honghong Yi[1,2] · Shunzheng Zhao[1,2] · Sani Zaharaddeen[1] · Runcao Zhang[1] · Ruijie Zhuang[1] · Yingli Ma[1]

Received: 16 April 2019 / Accepted: 12 July 2019 / Published online: 26 July 2019

Abstract

A series of MnO_x/ACF_N, Ce-MnO_x/ACF_N, and Fe-Ce-MnO_x/ACF_N catalysts on selective catalytic reduction (SCR) of NO_x with NH_3 at low-middle temperature had been successfully prepared through ultrasonic impregnation method, and the catalysts were characterized by SEM, XRD, BET, H_2-TPR, NH_3-TPD, XPS, and FT-IR spectroscopy, respectively. The results demonstrated that the 15 wt% $Fe_{(1)}$-$Ce_{(3)}$-$MnO_{x(7)}$/ACF_N catalyst achieved 90% NO_x conversion (100~300 °C), good water resistance, and stability (175 °C). The excellent catalytic performance of the $Fe_{(1)}$-$Ce_{(3)}$-$MnO_{x(7)}$/ACF_N catalyst was mainly attributed to the interaction among Mn, Ce, and Fe. The doping of Fe promoted the dispersion of Ce and Mn and the formation of more Mn^{4+} and chemisorbed oxygen on the surface of a catalyst. This work laid a foundation for the successful application of active carbon fiber in the field of industrial denitrification, especially in the aspect of denitrification moving bed.

Keywords Selective catalytic reduction · Low-middle temperature · Activated carbon fiber · Ce-MnO_x · Fe

Introduction

In recent years, the use of gas boilers with clean combustible natural gas or liquefied petroleum gas (as fuel source) is encouragingly used as replacement to gas boilers with coal during the winter-heating period in China and, practically, this led to the policy called "coal-to-gas policy." The main aim of this substitution is to reduce emission of nitrogen oxides (NO_x) and other pollutants from coal consumption. One of the main sources of stationary NO_x is the gas boilers with higher water vapor content, which resulted in many environmental problems including ozone hole, photochemical smog, and acid rain (Fan et al. 2018; Gao et al. 2017a; Zhang et al. 2017). Selective catalytic reduction (SCR) of NO_x with NH_3 has been industrially proven as the predominant method for post-combustion abatement of NO_x emissions. At present, commercial SCR catalysts (V_2O_5-WO_3/TiO_2) exhibit catalytic activity within a narrow temperature window (300~400 °C), and they are easily poisoned by a high concentration of SO_2 and dust (Marani et al. 2017; Sun et al. 2018a). The flue gas temperature behind desulfurization and dust wiper is ordinarily below 200 °C, which is beneficial to recover sensible heat and latent heat of water vapor condensation in the flue gas, thus improving the efficiency of the gas boiler. However, the actual flue gas temperature fluctuates so greatly that the catalysts need to maintain high catalytic activity over a relatively wide temperature range. Therefore, it is necessary to design and explore low-middle-temperature SCR catalysts (100~300 °C) (Gao et al. 2017b; Meng et al. 2018).

TiO_2, γ-Al_2O_3, molecular sieve, and carbon-based materials have been extensively studied as the supported catalyst carriers (Anthonysamy et al. 2018; Li et al. 2018a, 2018b; Wang et al. 2015; Wang et al. 2018). Compared to aluminum and titanium, carbon-based materials including activated carbon/coke, activated carbon fibers, carbon nanotubes, and graphenes have abundant oxygen-containing functional groups, which are beneficial for the adsorption of reactants such as NO_x and NH_3. And, large specific surface area makes the active and assistant components homogeneously dispersed on the surface, thereby providing more catalytic active sites

Responsible editor: Philippe Garrigues

✉ Xiaolong Tang
txiaolong@126.com

[1] Department of Environmental Engineering, School of Energy and Environmental Engineering, University of Science and Technology Beijing, Beijing 100083, People's Republic of China

[2] Beijing Key Laboratory of Resource-oriented Treatment of Industrial Pollutants, University of Science and Technology Beijing, Beijing 100083, People's Republic of China

(Fan et al. 2011; Grzybek et al. 2008). Activated carbon fibers (ACFs) are a flexible material in the form of silk, felt, cloth, etc. If it will be used as an industrial moving-bed denitration catalyst, the problem of wear and tear among the catalyst particles will be avoided. Transition metal oxides, especially manganese oxides (Sun et al. 2018b; Yan et al. 2018; Zhang et al. 2018) and cerium dioxide (Hu et al. 2018; Ma et al. 2018), have been proven to be effective for low-middle-temperature NH_3-SCR.

Liu et al. (2013) prepared MnCe catalysts by the surfactant template method, and 100% NO_x conversion (at 100~200 °C) was achieved by the best catalyst. The research proved that increasing the content of Mn is helpful to improve the low-temperature activity of the MnCe catalyst, and the doping of Ce can increase the N_2 selectivity. The appropriate proportion of the MnCe catalyst has the high surface area and the small active sites, which can promote the adsorption and activation of NH_3 and NO_x. Liu et al. (2018a) also found that the strong interaction between the different metals is benefited to improve the catalytic activity, and Ce easily interacts with other metals. The synergetic effect between Ce and Sn is favorable to enhance the redox property and increase the Lewis acidity, thus improving the NH_3-SCR performance of the Ce-Sn binary oxide catalyst. Moreover, a novel Ni-Ce-Ti–mixed oxide catalyst prepared by hydrothermal showed higher NH_3-SCR activity in a wide temperature range (250~450 °C). The synergetic effect between Ni and Ce can account for the excellent NH_3-SCR catalytic activity of the $Ni_{0.3}Ce_{0.1}Ti_{0.6}$ catalyst because of more oxygen vacancies and high redox property by the redox cycles ($Ni^{3+} + Ce^{3+} \leftrightarrow Ni^{2+} + Ce^{4+}$) (Liu et al. 2018b). Recently, ACFs as the carrier were studied widely for the low-middle-temperature NH_3-SCR, such as MnO_x/ACF (Lu et al. 2016; Wang et al. 2014), CeO_2/ACF (Lu et al. 2010; Zhu et al. 2011), and MnO_x-CeO_2/ACF (Li et al. 2015a, 2015b; Lu et al. 2016). Zhu et al. (2011) prepared the CeO_2/ACF_N catalyst that exhibited good catalytic activity, which obtained 94.0% NO conversion in the range of 150~270 °C. The MnO_x-CeO_x/ACF_N catalyst studied by Shen et al. (2008) showed the best catalytic activity (nearly 100% NO conversion) at 100~150 °C. It is worth noting that the modification of MnO_x-CeO_x/support catalysts by doping transition metals proved to improve catalytic activity such as Fe or Co doped Mn-Ce/TiO_2 catalyst (Xu et al. 2017; Shen et al. 2018). However, to the best knowledge of the authors, this research is among the very few publications on Fe-doped MnO_x-CeO_x/ACF_N catalysts for broadening its low-middle-temperature window.

In this work, the modified ACFs with nitric acid (40 wt%) which named ACF_N was used to prepare a series of MnO_x/ACF_N, M-MnO_x/ACF_N (M = Ce, Cu, Co, Cr, Ni, Fe), and Fe-Ce-MnO_x/ACF_N catalysts. The relationship between the surface property and catalytic activity of the catalysts was studied by means of scanning electron microscopy (SEM), X-ray diffraction (XRD), BET, H_2-TPR, NH_3-TPD, and X-ray photoelectron spectroscopy (XPS). Fourier transform infrared (FT-IR) spectroscopy was used to explore the effect of H_2O on the catalyst. The aim is to research the effect of transition metal on MnO_x/ACF_N and promote catalytic activity and water resistance of Ce-MnO_x/ACF_N catalysts by Fe doping at the different molar ratios of Fe/Ce for low-middle-temperature NH_3-SCR of NO_x. Thus, the successful application of activated carbon fibers in the field of industrial moving bed denitrification is realized.

Experimental section

Catalyst preparation

The rayon-based ACF (5 cm × 5 cm) pretreated with 40 wt% HNO_3 solution (noted as ACF_N) was used as the supporter, and the following analytical grade reagents: $Mn(CH_3COO)_2{\cdot}4H_2O$, $Ce(NO_3)_3{\cdot}6H_2O$, and $Fe(NO_3)_3{\cdot}9H_2O$ were used as the precursors of metal oxides to modified ACF_N. Firstly, the MnO_x/ACF_N was prepared via the ultrasonic impregnation method (Huang et al. 2008; Marbán et al. 2003; Shen et al. 2008). Meanwhile, the optimum mass load (0%, 10%, 15%, 20%) of the MnO_x/ACF_N and the calcination temperature (400 °C, 500 °C, 600 °C, in N_2 stream) were studied. Then, the MnO_x/ACF_N was modified with Ce at different Ce/Mn molar ratios and tested for SCR activity at low-middle temperature. Different doping elements (Cu, Co, Cr, Ni, and Fe) were screened with reference to the Ce/Mn optimal molar ratio. Finally, a trace amount of Fe-doped Ce-MnO_x/ACF_N catalysts was prepared and the optimum molar ratio was screened. The typical catalysts were investigated for improved SCR performances (activity and water resistance) at low-middle temperature.

Catalytic performance

The catalytic performance was evaluated by a quartz fix-bed continuous-flow reactor (i.d. 7 mm) containing 0.1 g of the catalyst. Each flue gas component was accurately controlled by a mass flow controller to ensure the total flow rate of 200 mL min^{-1}, corresponding to a mass hour space velocity that can be expressed as W/F = 0.5 mg (mL $min^{-1})^{-1}$. Meanwhile, the filling height of the catalyst is controlled to ensure that the gas volume space velocity is constant at 20,000 h^{-1}. The composition of reaction gas is as follows: 500 ppm NO, 500 ppm NH_3, 5 vol% O_2, and balance gas of N_2. The concentration of NO_x in inlet and outlet gas was analyzed by an online FT-IR spectrometer (iS50). The NO_x conversion was calculated as follows:

$$NO_{x_{conversion}}(\%) = \frac{[NO_x]_{in} - [NO_x]_{out}}{[NO_x]_{in}} \times 100 \quad (1)$$

$$N_2 \text{ selective } (\%) = \left(1 - \frac{2[N_2O]_{out}}{([NO_x]_{in} - [NO_x]_{out} + [NH_3]_{in} - [NH_3]_{out})}\right) \times 100 \quad (2)$$

$$[NO_x] = [NO] + [NO_2]$$

Catalyst characterization

A SU8010 electron microscope was used for the SEM. The specific surface area of the samples was analyzed for the Brunauer-Emmett-Teller (BET) method with an Autosorb-iQ. The crystal structure of the samples was analyzed by powder XRD using a TTR-III system with CuKα (λ = 0.154 nm) radiation, and the scanning range was 10~90° (2θ) with a 10° min^{-1} sampling interval. Temperature-programmed reduction with hydrogen (H_2-TPR) was performed using an Extrel MAX300 (Extrel, USA) apparatus, and the heating rate is 10 °C min^{-1}. Temperature-programmed desorption of ammonia (NH_3-TPD) was performed using the Extrel MAX300 (Extrel, USA) apparatus. The heating rate of the samples is 10 °C min^{-1}. XPS was measured at ambient temperature by a Thermo Scientific Escalab 250Xi using Al Kα radiation (hv = 1486.6 eV). FT-IR spectroscopy spectra results of the samples were obtained from a FT-IR spectrometer (iS50).

Results and discussion

NH_3-SCR performance

The NO_x conversion of X wt% MnO_x/ACF_N catalysts (X = 0, 10, 15, and 20) is shown in Fig. 1 a. The pure ACF_N was mostly inactive from 100 to 300 °C, where the best NO_x conversion of only 20.1% was observed at 150 °C. The higher NO_x conversion was about 60.0% at 175 °C for 10 wt% MnO_x/ACF_N. The 15 wt% MnO_x/ACF_N catalyst showed the best SCR activity, and the NO_x conversion was about 40.4% at 100 °C and increased to 80.7% at 175 °C, while the activity was reduced to 48.2% at a middle temperature of up to 300 °C. As the mass load increased to 20 wt%, the best SCR activity of 66.0% NO_x conversion was achieved at 175 °C. This phenomenon might result from the occupation of active sites and the blockage of surface pores over the overload MnO_x/ACF_N catalysts (Shen et al. 2008; Zhu et al. 2011). The SCR activity of 15 wt% MnO_x/ACF_N catalysts calcined at different temperature varied with the reaction temperature (100~300 °C) is shown in Fig. 1 b. The NO_x conversion of the sample calcined at 500 °C was higher than that of the other samples. In the reaction, the main reason for the deactivation of MnO_x/ACF_N catalysts is due to the incomplete decomposition of metal salts or the agglomeration of active oxides. Therefore, the proper calcination temperature is especially important for the catalytic activity of catalysts.

Thus, in the further studies, the optimum total mass load of metal oxides was set as 15% on the ACF_N catalyst, and the calcination temperature was optimized as 500 °C for 6 h in the stream of nitrogen.

Figure 2 a illustrates that the catalytic activity of Ce-MnO_x/ACF_N catalysts gradually increased with an increase of Mn/Ce ratio. The $Ce_{(3)}$-$MnO_{x(7)}/ACF_N$ catalyst showed good low-temperature activity at 100~200 °C, and up to 87.7% NO_x conversion at 175 °C was achieved. As reported by Wang et al. (2012), the presence of CeO_2 could not only promote the dispersion of MnO_x but also result in different oxidation states of manganese, which could be beneficial to improve the activity of the NH_3-SCR catalyst. Furthermore, the presence of CeO_2 in Mn-based catalysts could improve the oxygen storage capacity and oxygen mobility, thus facilitating the catalytic process via the *fast SCR*.

Figure 2 b shows the NO_x conversion of MnO_x/ACF_N catalysts doped with several elements based on the optimal molar ratio of Mn/Ce. As shown above, the Ce-MnO_x/ACF_N catalyst showed higher activity than other catalysts at low temperature, but its catalyst activity is poorer than that of others in the middle-temperature range. Fe-MnO_x/ACF_N and Cr-MnO_x/ACF_N catalysts had better SCR activity at middle temperature (200~300 °C). However, Cr is a highly toxic heavy metal, which has harmful effects on the human health and environment, so the use of chromium-containing catalysts is highly restricted.

Many studies had found that FeO_x as the main active component or auxiliary agent of SCR denitration catalyst can remarkably improve catalytic activity (Xu et al. 2017). Two ways were used to control the molar amount of doped Fe for broadening the temperature window of the Ce-MnO_x/ACF_N catalyst. One way was to adjust the doping amount of Ce and Fe on the basis of constant Mn molar number. As shown in Fig. 3 a, the change trend of $Fe_{(0.5)}$-$Ce_{(2.5)}$-$MnO_{x(7)}/ACF_N$, $Fe_{(1)}$-$Ce_{(2)}$-$MnO_{x(7)}/ACF_N$, and $Fe_{(2)}$-$Ce_{(1)}$-$MnO_{x(7)}/ACF_N$ was similar, and as compared to $Ce_{(3)}$-$MnO_{x(7)}/ACF_N$, the catalysts showed well-broadening catalytic activity which was about 85.4% at 200 °C. Another way was to add trace Fe on the premise that the doping amount of Mn and Ce remains unchanged; as shown in Fig. 3 b, $Fe_{(0.5)}$-$Ce_{(3)}$-$MnO_{x(7)}/ACF_N$ has good low temperature performance, but its catalytic performance is poor at middle temperature. The $Fe_{(1)}$-$Ce_{(3)}$-$MnO_{x(7)}/ACF_N$ catalyst showed 90.8% NO_x conversion at 175 °C, which was only increased by 3.1% than $Ce_{(3)}$-$MnO_{x(7)}/ACF_N$, but the catalytic performance at the middle-temperature (200~300 °C) level was significantly improved. On the basis of $Fe_{(1)}$-$Ce_{(3)}$-$MnO_{x(7)}/ACF_N$, any increase or decrease in the amount of Fe doping did not widen the catalyst temperature window. It is proved that Fe-modified Ce-MnO_x/ACF_N catalysts could enhance its catalytic activity

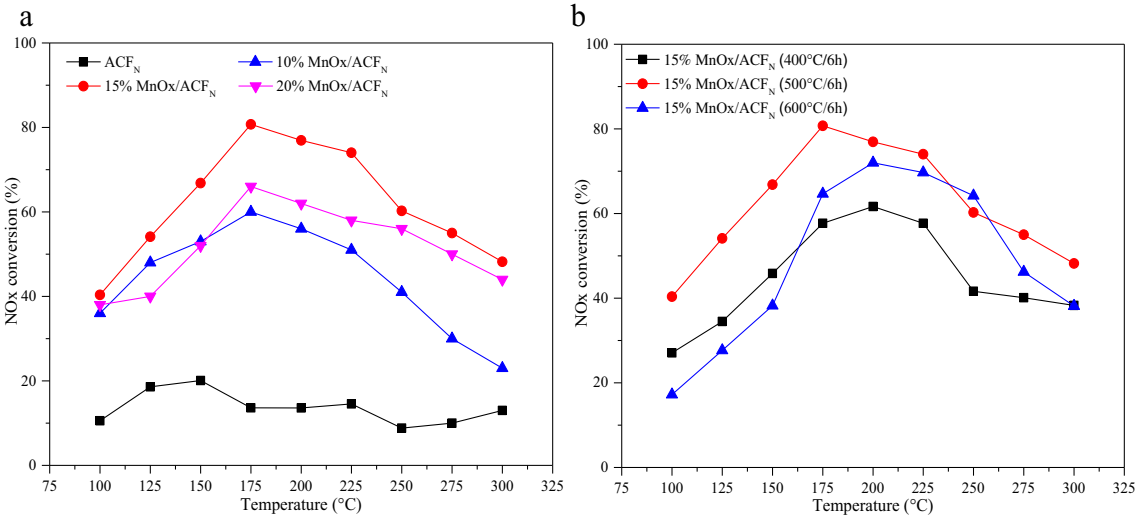

Fig. 1 NO_x conversion of MnO_x/ACF_N with different (**a**) mass loadings and (**b**) calcination temperatures. Reaction conditions: [NO] = [NH_3] = 500 ppm, [O_2] = 5%, W/F = 0.5 mg (mL $min^{-1})^{-1}$, and a flue rate of 200 mL min^{-1} in N_2 balance gas

at the low-middle temperature for NH_3-SCR selectivity of NO_x.

Figure 4 a compares the NO_x conversion of MnO_x/ACF_N, $Ce_{(3)}$-$MnO_{x(7)}/ACF_N$, and $Fe_{(1)}$-$Ce_{(3)}$-$MnO_{x(7)}/ACF_N$ catalysts. It could be seen from Fig. 4 a that the addition of Ce availably promoted the activity of the MnO_x/ACF_N catalyst from 100 to 200 °C. Further doping of trace Fe could obviously enhance the NO_x conversion of the $Ce_{(3)}$-$MnO_{x(7)}/ACF_N$ catalyst in the middle-temperature range (200~300 °C), thereby widening the temperature window of the $Fe_{(1)}$-$Ce_{(3)}$-$MnO_{x(7)}/ACF_N$ catalyst. Figure 4 b shows the N_2 selectivity of MnO_x/ACF_N, $Ce_{(3)}$-$MnO_{x(7)}/ACF_N$, and $Fe_{(1)}$-$Ce_{(3)}$-$MnO_{x(7)}/ACF_N$ catalysts. It was found that the N_2 selectivity decreased with the increase of temperature. Throughout the temperature range, the $Fe_{(1)}$-$Ce_{(3)}$-$MnO_{x(7)}/ACF_N$ catalyst showed good N_2 selectivity. It can be concluded that the $Fe_{(1)}$-$Ce_{(3)}$-$MnO_{x(7)}/ACF_N$ catalyst not only possesses high De-NO_x property but also has high N_2 selectivity.

SEM and XRD analysis

Figure 5 shows SEM images of the samples, in which the ACF_N was uniformly decorated with metal oxides. As shown in Fig. 5 a, the surface of ACF_N was smooth and clean, which proved that nitric acid treatment could remove impurities from the ACF_N surface. After loading Mn, Ce, and Fe oxides, the ACF_N surface became rougher (Fig. 5b–d). For MnO_x/ACF_N, the surface of ACF_N had some agglomerations of MnO_x, which might be relevant to incomplete modification (Fig. 5b) (Zhu et al. 2011). For $Ce_{(3)}$-$MnO_{x(7)}/ACF_N$ and $Fe_{(1)}$-$Ce_{(3)}$-$MnO_{x(7)}/ACF_N$, active phases were well dispersed on the surface of ACF_N, which indicated that the doping of Ce

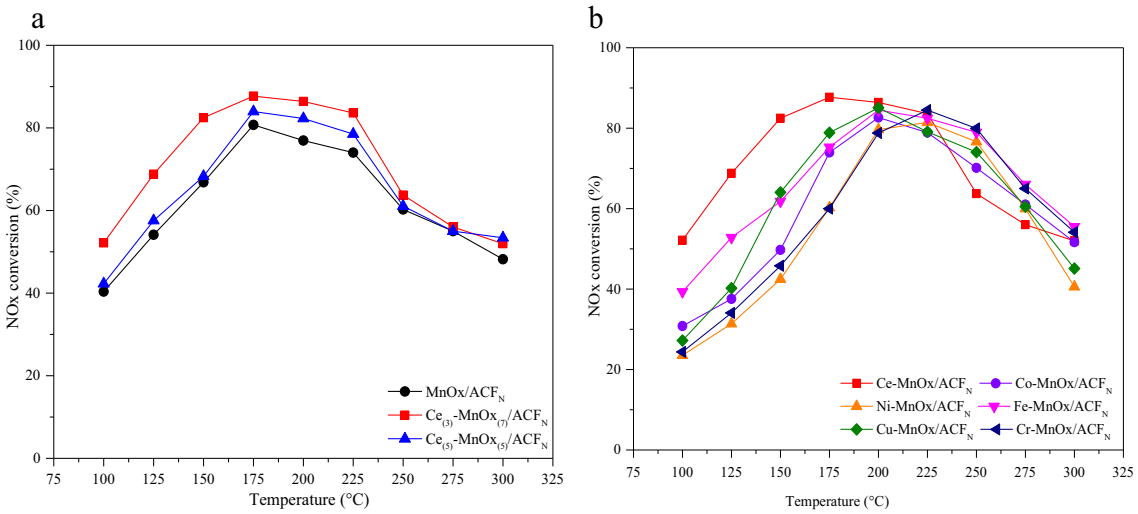

Fig. 2 NO_x conversion of **a** Ce-MnO_x/ACF_N with different molar ratios and **b** M-MnO_x/ACF_N (M = Ce, Co, Ni, Fe, Cu, Cr) based on Mn/Ce = 7:3. Reaction conditions: [NO] = [NH_3] = 500 ppm, [O_2] = 5%, W/F = 0.5 mg (mL $min^{-1})^{-1}$, and a flue rate of 200 mL min^{-1} in N_2 balance gas

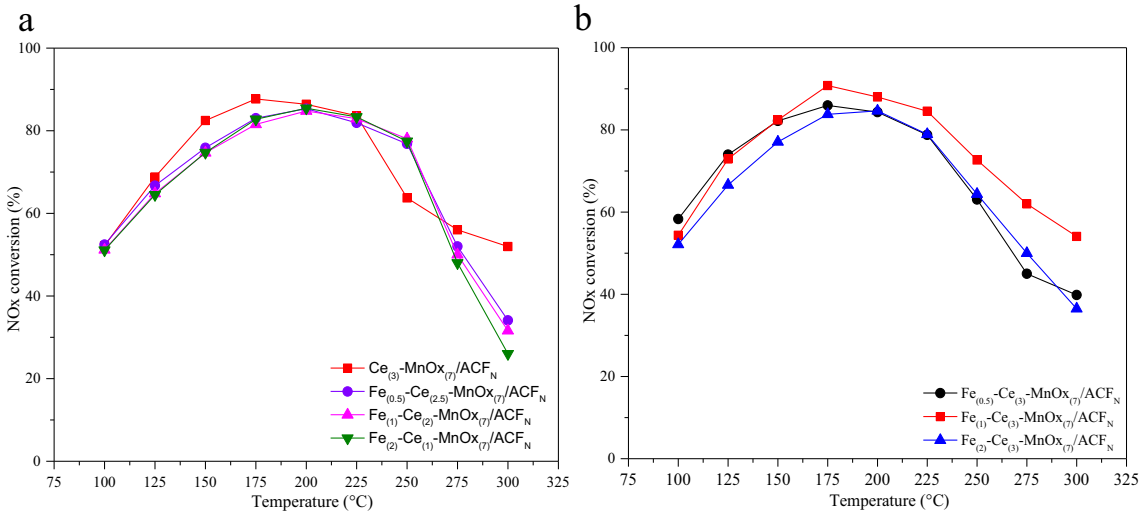

Fig. 3 NO_x conversion of **a** Fe-Ce-MnO_x/ACF_N catalysts with different molar ratios of Ce and Fe and **b** $Fe_{(x)}$-$Ce_{(3)}$-$MnO_{x(7)}$/ACF_N catalysts (x = 0.5, 1, 2). Reaction conditions: [NO] = [NH_3] = 500 ppm, [O_2] = 5%, W/F = 0.5 mg (mL $min^{-1})^{-1}$, and a flue rate of 200 mL min^{-1} in N_2 balance gas

and Fe contributed to dispersion of active components (Fig. 5c, d), but there were still some larger particles in the former. As compared to the MnO_x/ACF_N and $Ce_{(3)}$-$MnO_{x(7)}$/ACF_N catalysts, the $Fe_{(1)}$-$Ce_{(3)}$-$MnO_{x(7)}$/ACF_N catalyst showed more apparent uniform and fine particles adhering to the surface of the catalyst, which resulted in the good catalytic activity of the catalyst.

The powder X-ray diffraction patterns of ACF_N, MnO_x/ACF_N, $Ce_{(3)}$-$MnO_{x(7)}$/ACF_N, and $Fe_{(1)}$-$Ce_{(3)}$-$MnO_{x(7)}$/ACF_N catalysts in the 2θ range of 10°–90° are shown in Fig. 6. For the ACF_N, the intense and sharp diffractions at 23.9° and 43.8° could be primarily attributed to graphite charcoal (Zhu et al. 2011), which indicated that ACF_N is highly graphitized. After loading MnO_x, the peak intensity of graphite became small and flattened, which illustrated that there was a strong interaction of MnO_x and ACF_N (Lu et al. 2015). The interaction between MnO_x and CeO_2 was stronger, so the diffraction peaks of graphite were also detected on the $Ce_{(3)}$-$MnO_{x(7)}$/ACF_N catalyst. The diffraction peaks corresponding to the CeO_2 were detected on the surface of $Ce_{(3)}$-$MnO_{x(7)}$/ACF_N and $Fe_{(1)}$-$Ce_{(3)}$-$MnO_{x(7)}$/ACF_N catalysts at 29.1° and 57.2°, respectively (Chang et al. 2012), but the MnO_x and FeO_x diffraction peaks did not appeared, which implies that the metal oxides were well distributed on the surface of the support. The above conclusion is also proved by SEM images (Fig. 5).

BET analysis

Figure 7 a shows the nitrogen adsorption-desorption isotherms of the samples. All the adsorption isotherm curves exhibited type I, and there was no obvious hysteresis loop on the basis of the IUPAC classification (Thommes et al. 2015), which suggested that they were predominantly

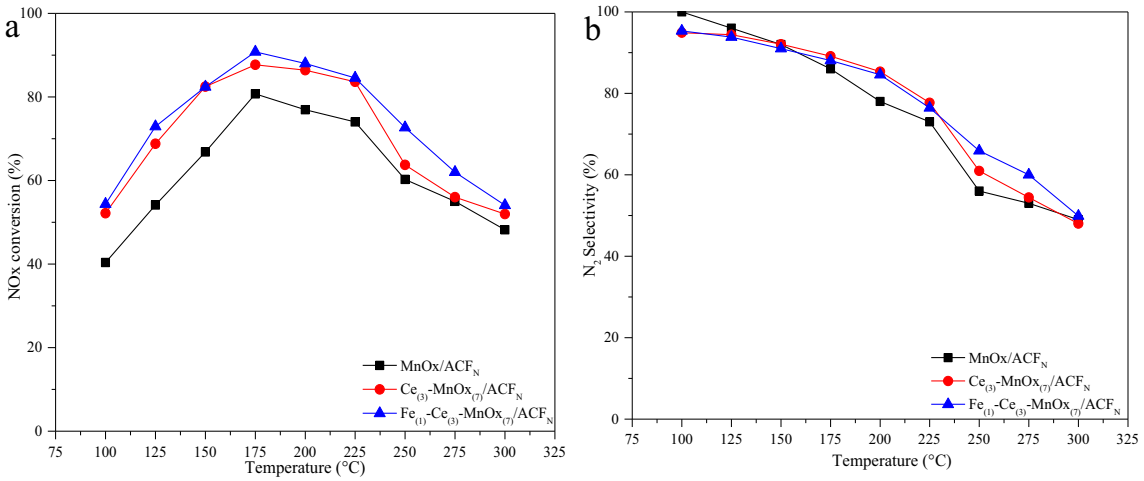

Fig. 4 **a** NO_x conversion and **b** N_2 selectivity of MnO_x/ACF_N, $Ce_{(3)}$-$MnO_{x(7)}$/ACF_N, and $Fe_{(1)}$-$Ce_{(3)}$-$MnO_{x(7)}$/ACF_N catalysts. Reaction conditions: [NO] = [NH_3] = 500 ppm, [O_2] = 5%, W/F = 0.5 mg (mL $min^{-1})^{-1}$, and a flue rate of 200 mL min^{-1} in N_2 balance gas

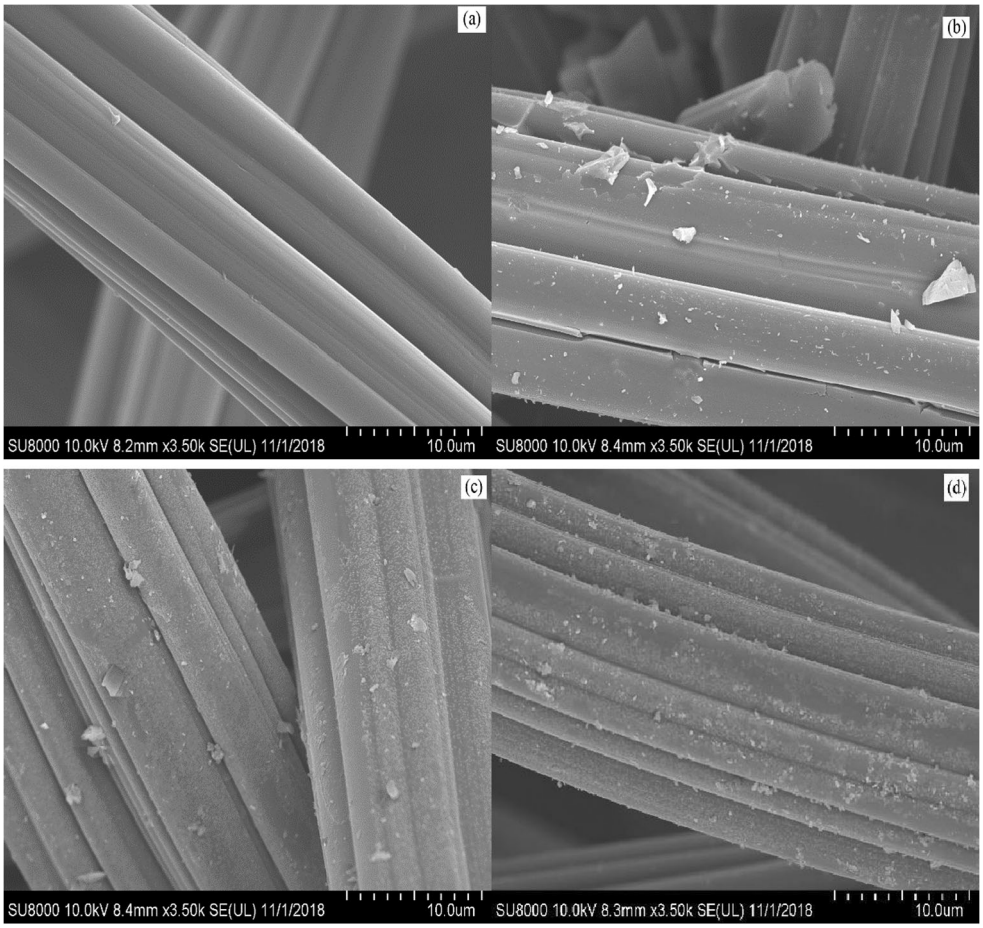

Fig. 5 SEM images of the catalysts. **a** ACF_N. **b** MnO_x/ACF_N. **c** $Ce_{(3)}$-$MnO_{x(7)}/ACF_N$. **d** $Fe_{(1)}$-$Ce_{(3)}$-$MnO_{x(7)}/ACF_N$

microporous materials. The surface areas and pore parameters of ACF, ACF_N, MnO_x/ACF_N, $Ce_{(3)}$-$MnO_{x(7)}/ACF_N$, and $Fe_{(1)}$-$Ce_{(3)}$-$MnO_{x(7)}/ACF_N$ catalysts are listed in Table 1, which shows that the surface area of all catalysts is above 1000 $m^2\ g^{-1}$. Figure 7 b illustrates the pore diameter distribution of all the samples. As shown in Table 1, the nitric acid modification could increase the micropore surface area (S_{micro}) but reduce the external surface area ($S_{external}$) and mesopore surface area (S_{meso}) obviously. When ACF_N supported the Mn, Ce, and Fe, the S_{BET} and S_{micro} of MnO_x/ACF_N, $Ce_{(3)}$-$MnO_{x(7)}/ACF_N$, and $Fe_{(1)}$-$Ce_{(3)}$-$MnO_{x(7)}/ACF_N$ declined in different degrees, which might be due to the dispersion of metal oxide species on the surface of the carrier or micropore which was blocked by the metal species (Huang et al. 2008; Zhu et al. 2011), while the $Fe_{(1)}$-$Ce_{(3)}$-$MnO_{x(7)}/ACF_N$ catalyst exhibited better low-middle-temperature SCR performance, probably due to the abundant micropores in the catalyst. As it can be seen from Table 1, doping of Fe enlarged the micropore-specific surface area and micropore volume of the $Fe_{(1)}$-$Ce_{(3)}$-$MnO_{x(7)}/ACF_N$ catalyst, thereby improving the low-middle-temperature SCR activity.

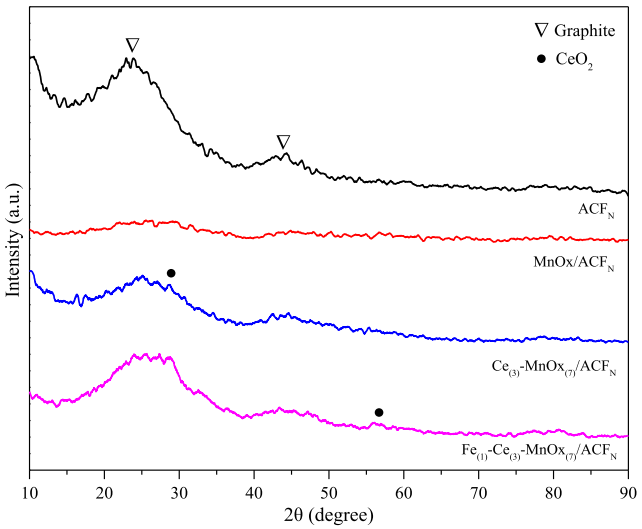

Fig. 6 XRD patterns of the ACF_N, MnO_x/ACF_N, $Ce_{(3)}$-$MnO_{x(7)}/ACF_N$, and $Fe_{(1)}$-$Ce_{(3)}$-$MnO_{x(7)}/ACF_N$ catalysts

H_2-TPR analysis

The oxidation states of MnO_x/ACF_N, $Ce_{(3)}$-$MnO_{x(7)}/ACF_N$, and $Fe_{(1)}$-$Ce_{(3)}$-$MnO_{x(7)}/ACF_N$ catalysts are shown

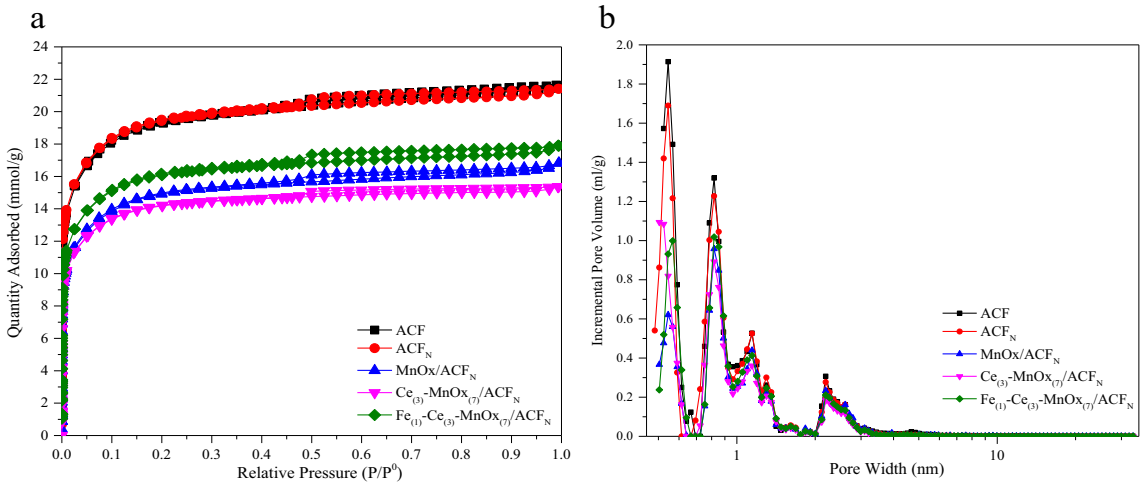

Fig. 7 **a** Nitrogen adsorption-desorption isotherms. **b** Corresponding pore diameter distribution obtained by the DFT of ACF, ACF_N, MnO_x/ACF_N, $Ce_{(3)}$-$MnO_{x(7)}/ACF_N$, and $Fe_{(1)}$-$Ce_{(3)}$-$MnO_{x(7)}/ACF_N$ catalysts

in Fig. 8. MnO_x/ACF_N showed three reduction peaks at 341 °C, 422 °C, and 480 °C, corresponding to $MnO_2 \rightarrow Mn_2O_3$, $Mn_2O_3 \rightarrow Mn_3O_4$, and $Mn_3O_4 \rightarrow MnO$, respectively (Chen et al. 2016; Ramesh et al. 2008; Tian et al. 2011). For the $Ce_{(3)}$-$MnO_{x(7)}/ACF_N$ catalyst, the peak at 335 °C could be regarded as the transformation of $MnO_2 \rightarrow Mn_2O_3$, the peak at 424 °C belonged to $Mn_2O_3 \rightarrow Mn_3O_4$, and the peak around 489 °C was regarded as the reduction of $Mn_3O_4 \rightarrow MnO$ (Fang et al. 2017). And, the reduction peak from 520 to 670 °C was classified to $CeO_2 \rightarrow Ce_2O_3$, consisting with the description of Liu et al. (2014). For the $Fe_{(1)}$-$Ce_{(3)}$-$MnO_{x(7)}/ACF_N$ catalyst, the peak at 337 °C and 415 °C could be attributed to the change of $MnO_2 \rightarrow Mn_2O_3$ and $Mn_2O_3 \rightarrow Mn_3O_4$, respectively (Cao et al. 2015; Fang et al. 2017; Li et al. 2015a, 2015b). The peak centered at 708 °C was ascribed to the process of $Fe_3O_4 \rightarrow FeO$ (France et al. 2017). Compared with the other catalysts, the reduction peaks of MnO_x shifted to lower-temperature regions, Zuo et al. (2009) thought that it was due to the good dispersion and tiny crystal size of MnO_x. In addition, the $Fe_{(1)}$-$Ce_{(3)}$-$MnO_{x(7)}/ACF_N$ catalyst showed the largest H_2 consumption than the $Ce_{(3)}$-$MnO_{x(7)}/ACF_N$ catalyst followed by the MnO_x/ACF_N catalyst in the whole reaction temperature. It is concluded that the former exposed more reductive species, thus improving the redox ability of the catalyst (Gao et al. 2019). The doping of Fe can promote the formation of more surface-chemisorbed oxygen, thereby contributing to low-middle-temperature catalytic activity of the catalysts (Ma et al. 2018; Tang et al. 2016). This H_2-TPR result is consistent with the XPS (Fig. 10).

NH_3-TPD analysis

The adsorption and activation of NH_3 on the surface acid sites of catalysts are viewed as a major process in NH_3-SCR reaction (Zhang et al. 2013). The surface acidity and strength of the catalysts obtained from NH_3-TPD curves are shown in Fig. 9. All the catalysts showed at least two desorption peaks. The NH_3 desorption amounts of different catalysts are shown in Table 2. According to relevant literatures, the peaks around 100~200 °C were attributed to the ammonia which was physically adsorbed in the weak acid sites, the peaks at 200~500 °C led to NH_3 desorption on the medium acidic sites, and the peaks above 500 °C were assigned to NH_3 desorption on the strong acidic sites (Jiang et al. 2018; Xu et al. 2017). As shown in Table 2, the $Fe_{(1)}$-$Ce_{(3)}$-$MnO_{x(7)}/ACF_N$ catalyst revealed the much larger area, especially at the high-temperature region, indicating the presence of abundant acid sites on the surface of

Table 1 N_2 adsorption and desorption results

Sample	S_{BET} (m^2 g^{-1})	S_{micro} (m^2 g^{-1})	$S_{external}$ (m^2 g^{-1})	S_{meso} (m^2 g^{-1})	V_t (cm^3 g^{-1})	V_{mi} (cm^3 g^{-1})	V_{me} (cm^3 g^{-1})	D_A (nm)
ACF	1615.4	1481.9	133.5	77.6	0.75	0.62	0.09	1.86
ACF_N	1633.2	1515.4	117.9	70.7	0.74	0.63	0.08	1.82
MnO_x/ACF_N	1238.3	1096.8	141.5	60.0	0.58	0.46	0.08	1.88
$Ce_{(3)}$-$MnO_{x(7)}/ACF_N$	1191.7	1093.3	98.5	42.1	0.53	0.45	0.05	1.79
$Fe_{(1)}$-$Ce_{(3)}$-$MnO_{x(7)}/ACF_N$	1347.6	1224.3	123.3	63.7	0.62	0.51	0.07	1.84

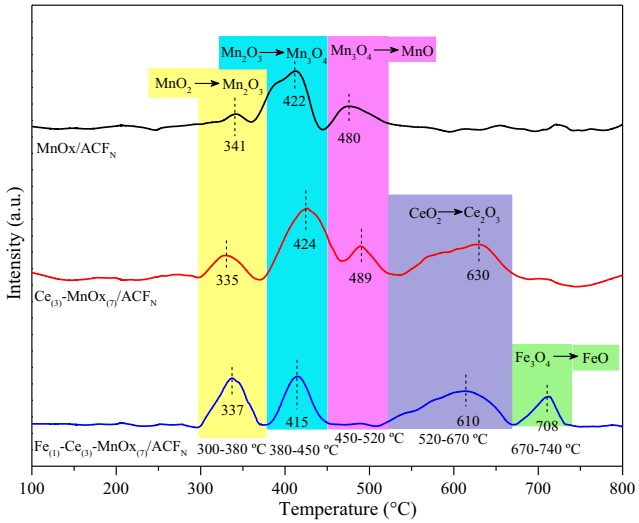

Fig. 8 H_2-TPR profiles of the MnO_x/ACF_N, $Ce_{(3)}$-$MnO_{x(7)}/ACF_N$, and $Fe_{(1)}$-$Ce_{(3)}$-$MnO_{x(7)}/ACF_N$ catalysts

the catalyst. The NH_3-TPD results demonstrated that doping Fe enhanced strong acid amount, which may be favorable to the NH_3-SCR reaction (Cao et al. 2015). Strong acid sites were dominant on the surface of $Fe_{(1)}$-$Ce_{(3)}$-$MnO_{x(7)}/ACF_N$ catalysts.

XPS analysis

The different XPS spectra of Mn 2*p*, Ce 3*d*, Fe 2*p*, and O 1*s* are shown in Fig. 10, and the surface relative atomic ratios of Mn, Ce, Fe, and O are shown in Table 3.

From Fig. 10 a, Mn 2*p* spectra have two peaks including Mn $2p_{1/2}$ and Mn $2p_{3/2}$. By performing peak-fitting deconvolutions, the Mn $2p_{3/2}$ spectra were divided into Mn^{2+} (641.2 eV ± 0.1 eV), Mn^{3+} (642.5 eV ± 0.1 eV), and

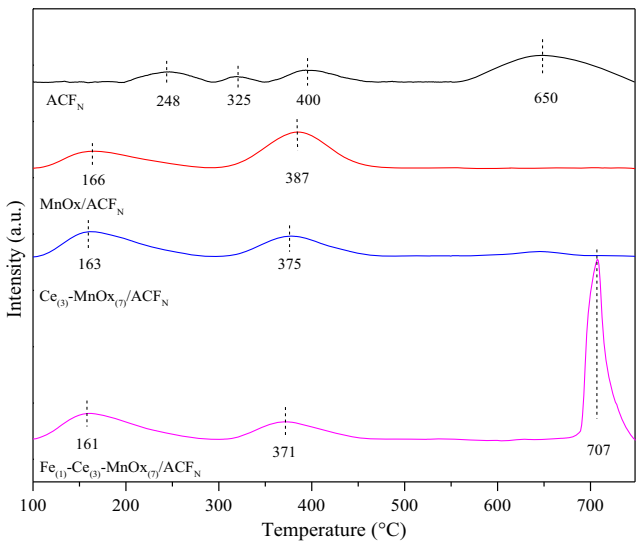

Fig. 9 NH_3-TPD profiles of the ACF_N, MnO_x/ACF_N, $Ce_{(3)}$-$MnO_{x(7)}/ACF_N$, and $Fe_{(1)}$-$Ce_{(3)}$-$MnO_{x(7)}/ACF_N$ catalysts

Mn^{4+} (645.0 eV ± 0.2 eV) (You et al. 2017; Zhou et al. 2016). From Table 2, the relative atomic ratio of Mn^{4+} increased from 47.6% of MnO_x/ACF_N to 48.6% of $Ce_{(3)}$-$MnO_{x(7)}/ACF_N$. After doping with Fe, the relative atomic ratio of Mn^{4+} increased to 53.1% of $Fe_{(1)}$-$Ce_{(3)}$-$MnO_{x(7)}/ACF_N$. From the H_2-TPR result shown in Fig. 8, it was generally thought that Mn^{4+} was propitious to the transformation of NH_3 to NH_2 (Wan et al. 2014). Cao et al. (2014) reflected that the coexistence of Mn^{4+} and Mn^{3+} could promote the catalytic activity of catalysts. It could prove that doping of Fe could provide a positive impact on increasing the relative content of Mn^{4+}, thereby accelerating the NH_3-SCR reaction.

The XPS spectra of Ce 3*d* are obtained in Fig. 10 b, which mainly contained the Ce $3d_{3/2}$ and Ce $3d_{5/2}$ spectra. The result indicated that Ce 3*d* orbit was represented by the multiple of *v* and *u*. The *v*, *v*″, and *v*‴ and *u*, *u*″, and *u*‴ peaks belonged to Ce^{4+} species, and *v*′ and *u*′ belonged to Ce^{3+} species (Sun et al. 2018c). From these peaks, it showed that the $Fe_{(1)}$-$Ce_{(3)}$-$MnO_{x(7)}/ACF_N$ catalyst was mainly in the Ce^{4+} oxidation state and Ce^{4+} and Ce^{3+} coexist on the catalyst surface. It was reported that the Ce^{4+} could promote the oxygen storage and release by the valence state transformation of Ce^{3+} and Ce^{4+} (Lu et al. 2018). After doping of Ce, the content of Mn^{4+} and Ce^{4+} increased, while the doping of Fe had a little effect on the valence changes of Ce.

The Fe 2*p* spectra of the $Fe_{(1)}$-$Ce_{(3)}$-$MnO_{x(7)}/ACF_N$ catalyst are shown in Fig. 10 c. By peak-fitting deconvolution, the spectrum peaks of Fe $2p_{3/2}$ and Fe $2p_{1/2}$ located at 710.5 eV, 715.1 eV, and 722.1 eV are attributed to Fe^{3+} (Li et al. 2015a, 2015b). In addition, the Fe^{2+} peaks (712.6 eV) are presented in the Fe $2_{p3/2}$ peak. As shown in Table 3, Fe^{3+} is the main present form of Fe element with a relative surface content of 76.7%. The result was consistent with H_2-TPR profiles (Fig. 8). The strong interaction between Fe and Mn led to the change of Fe^{2+} and Fe^{3+}, which promoted the generation of oxygen vacancy on the surface of the catalysts, thereby facilitating the low-middle SCR activity (Lu et al. 2018).

O 1*s* XPS spectrum is shown in Fig. 10 d. The peak at 529.8 eV ± 0.2 eV belonged to lattice oxygen (O_β); the peak at 531.3 eV ± 0.1 eV was part of chemisorbed oxygen and weakly bonded oxygen species (O_α); the binding energy of 533.0 eV ± 0.1 eV was considered to be oxygen in surface-adsorbed water species (O_γ). Table 3 shows the relative atomic ratio of oxygen species calculated through the peak area. The content of O_β in $Ce_{(3)}$-$MnO_{x(7)}/ACF_N$ (26.7%) was higher than that in MnO_x/ACF_N (12.3%). Ce doping not only improved the redox performance of the MnO_x/ACF_N catalyst but also facilitated the adsorption-desorption reversible cycle of O_β. The concentration of O_α in $Fe_{(1)}$-$Ce_{(3)}$-$MnO_{x(7)}/ACF_N$ (46.5%) was higher than that in MnO_x/ACF_N (39.0%) and $Ce_{(3)}$-$MnO_{x(7)}/ACF_N$ (35.8%), while the concentration of O_β decreased to 14.6%. Studies have shown that surface-chemisorbed oxygen was more active owing to the higher

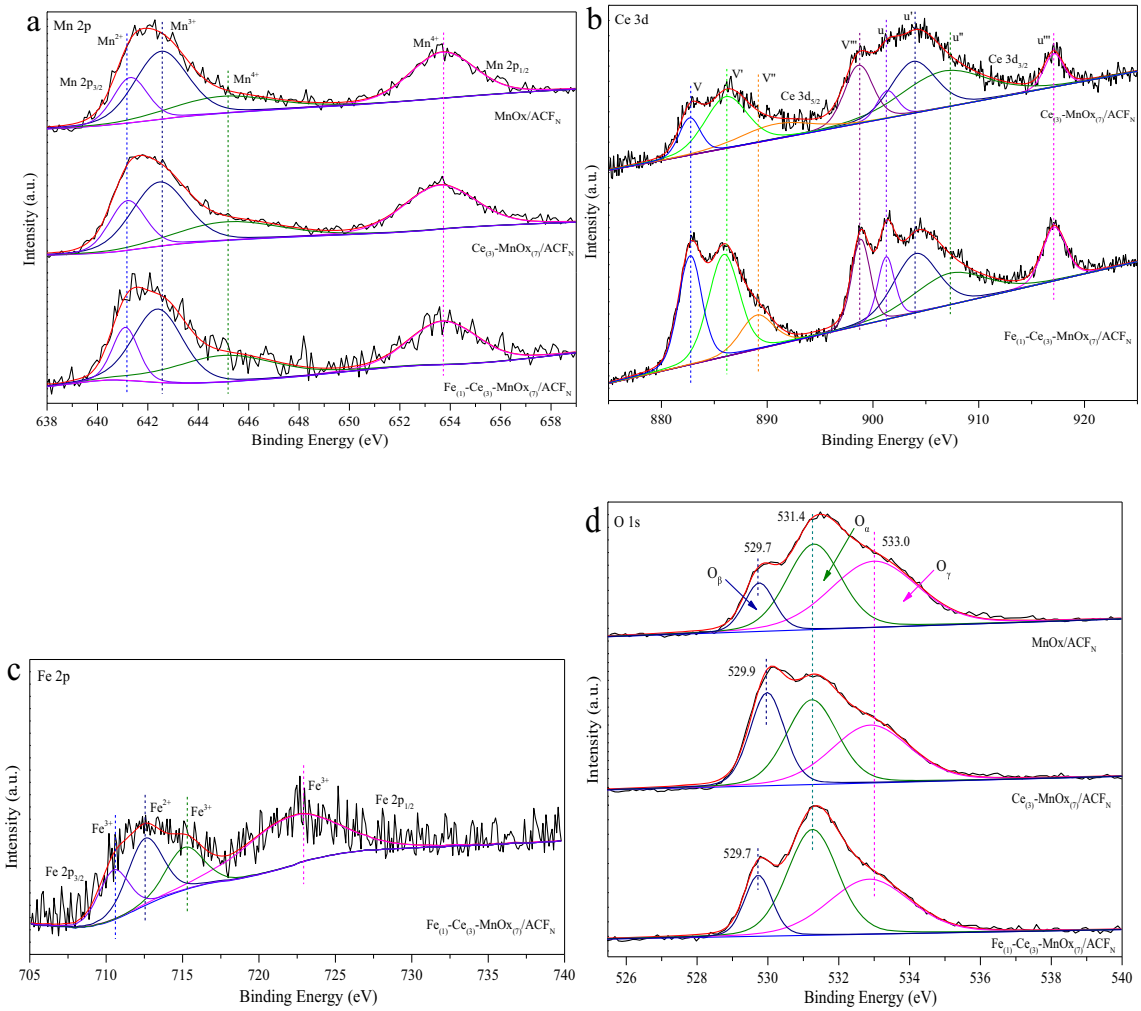

Fig. 10 XPS spectra of catalysts. **a** Mn 2*p*. **b** Ce 3*d*. **c** Fe 2*p*. **d** O 1*s*

mobility (Jiang et al. 2018; Zhang et al. 2013). The high concentration of chemisorbed oxygen can promote the redox cycle and enhance the oxidation of NO to NO_2 (Cao et al. 2015; Shen et al. 2017). Through above analysis, it is found that Fe had a positive effect on the transformation of gas-phase oxygen to chemisorbed oxygen.

The water resistance and stability of the catalysts

The gas boiler is one of the main sources of stationary NO_x, which has low smoke temperature and higher water vapor content. The exhaust flue gas emitted from the gas boiler containing water vapor (H_2O) is one of the important factors leading to the poisoning of catalysts at low-middle temperature. Figure 11 shows the NO_x conversion of MnO_x/ACF_N, $Ce_{(3)}$-$MnO_{x(7)}/ACF_N$, and $Fe_{(1)}$-$Ce_{(3)}$-$MnO_{x(7)}/ACF_N$ catalysts in the existence of 10 vol% H_2O. Before getting into the H_2O resistance test, the catalytic activity was maintained at 175 °C for 40 min. The NO_x conversion of MnO_x/ACF_N, $Ce_{(3)}$-$MnO_{x(7)}/ACF_N$, and $Fe_{(1)}$-$Ce_{(3)}$-$MnO_{x(7)}/ACF_N$ catalysts was 80.0%, 87.2%, and 90.5%, respectively. When 10 vol% H_2O was added into the flue gas, the NO_x conversion immediately decreased to 60.0%, 68.1%, and 76.0% for the MnO_x/ACF_N, $Ce_{(3)}$-$Mn_{(7)}/ACF_N$, and $Fe_{(1)}$-$Ce_{(3)}$-$MnO_{x(7)}$/

Table 2 The NH_3 desorption amount of different catalysts

Catalysts	NH_3 desorption amount (mmol g^{-1})			
ACF_N	0.24 (248 °C)	0.07 (325 eV)	0.30 (400 °C)	1.31 (650 °C)
MnO_x/ACF_N	0.68 (166 °C)	–	1.28 (387 °C)	–
$Ce_{(3)}$-$MnO_{x(7)}/ACF_N$	0.94 (163 °C)	–	0.70 (375 °C)	–
$Fe_{(1)}$-$Ce_{(3)}$-$MnO_{x(7)}/ACF_N$	1.02 (161 °C)	–	0.60 (371 °C)	1.88 (707 °C)

Table 3 XPS analysis of catalyst surface elements

Catalysts	Relative atomic ratio (%)									
	Mn 2*p*			Ce 3*d*		Fe 2*p*		O 1*s*		
	Mn^{4+}	Mn^{3+}	Mn^{2+}	Ce^{4+}	Ce^{3+}	Fe^{3+}	Fe^{2+}	O_α	O_β	O_γ
MnO_x/ACF_N	47.6	36.5	15.9	–	–	–	–	39.0	12.3	48.8
$Ce_{(3)}$-$MnO_{x(7)}/ACF_N$	48.6	34.0	17.4	63.4	36.6	–	–	35.8	26.7	37.5
$Fe_{(1)}$-$Ce_{(3)}$-$MnO_{x(7)}/ACF_N$	53.1	33.9	13.0	63.1	36.9	76.7	23.3	46.5	14.6	38.9

ACF_N catalysts in 5.5 h, respectively. The H_2O was removed from the flue gas after undergoing 5.5 h, and the catalytic activity of the catalysts was recovered to its the original level. The H_2O exhibited a reversible effect on the activities of the catalysts. It is possible that H_2O had the competitive adsorption with NH_3, which lead to a decrease in catalytic performance (Tang et al. 2018). Figure 12 presents the difference of functional groups in the fresh $Fe_{(1)}$-$Ce_{(3)}$-$MnO_{x(7)}/ACF_N$ catalyst and H_2O-resisted $Fe_{(1)}$-$Ce_{(3)}$-$MnO_{x(7)}/ACF_N$ catalyst. The band at 3440 cm^{-1} belonged to the surface –OH group, which proved the presence of H_2O (Wu et al. 2007). The band around 1640 cm^{-1} was caused by the surface C=O species. The band around 1199 cm^{-1} was attributed to the coordinated NH_3 on Lewis acid sites (Li et al. 2018a, 2018b). It is obviously found that the peak around 1199 cm^{-1} became weaker after the introduction of H_2O, which indicated the competitive adsorption between Lewis NH_3 and H_2O. The band at 1400 cm^{-1} was assigned to NH_4^+ adsorbed on Brønsted acid sites (Yu et al. 2017). The intensity of NH_4^+ peak became strong when H_2O was injected into the gas, indicating that the introduction of H_2O brought about more NH_3 absorbed in Brønsted acid sites. Meanwhile, it can be found that the peak intensity at 1400 cm^{-1} just increased slightly, so it is inferred that the addition of Fe slowed down the interaction between H_2O and Brønsted acid sites, thus improving the water resistance of the $Fe_{(1)}$-$Ce_{(3)}$-$MnO_{x(7)}/ACF_N$ catalyst.

The stability of catalysts has an important application value in the field of practical industrial denitration, so we conducted the stability test of the $Fe_{(1)}$-$Ce_{(3)}$-$MnO_{x(7)}/ACF_N$ catalyst, and Fig. 13 depicts the test result at 175 °C. The NO_x conversion maintained a stable level of about 90.0% during the tested 10 h and then decreased slightly. It is speculated that the stability was closely related to the surface properties of catalysts.

Conclusion

The metal doping type and molar ratio have a significant impact on the NH_3-SCR activity of catalysts. For Ce-MnO_x/ACF_N catalysts, the doping of Fe significantly broadened the temperature window of catalysts. Excellent catalytic performance of the $Fe_{(1)}$-$Ce_{(3)}$-$MnO_{x(7)}/ACF_N$ catalyst mainly attributed to the interaction among Mn, Ce, and Fe. A high concentration of Mn^{4+}, Ce^{4+}, Fe^{3+}, and chemisorbed oxygen can enhance catalytic activity. The characterization results

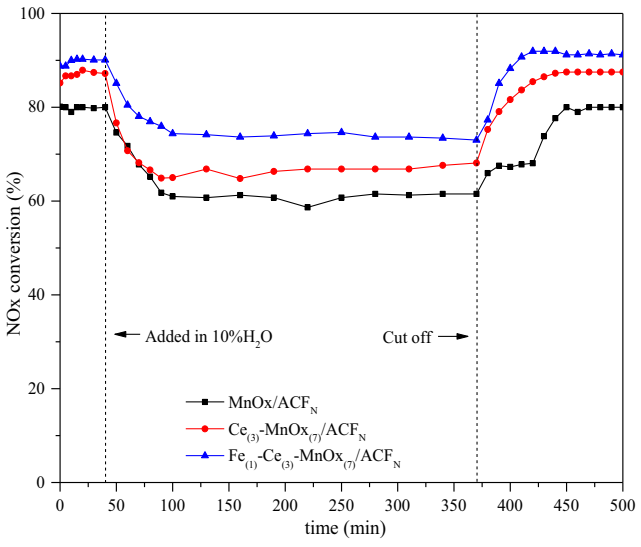

Fig. 11 The water resistance of the MnO_x/ACF_N, $Ce_{(3)}$-$MnO_{x(7)}/ACF_N$, and $Fe_{(1)}$-$Ce_{(3)}$-$MnO_{x(7)}/ACF_N$ catalysts. Reaction conditions: [NO] = [NH_3] = 500 ppm, [O_2] = 5%, 10 vol% H_2O, W/F = 0.5 mg (mL $min^{-1})^{-1}$, and a flue rate of 200 mL min^{-1} in N_2 balance gas

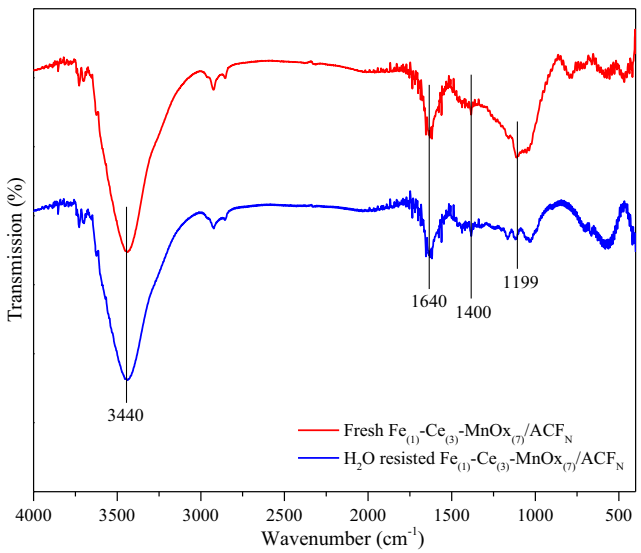

Fig. 12 FI-IR spectra of the fresh and H_2O-resisted $Fe_{(1)}$-$Ce_{(3)}$-$MnO_{x(7)}/ACF_N$ catalyst

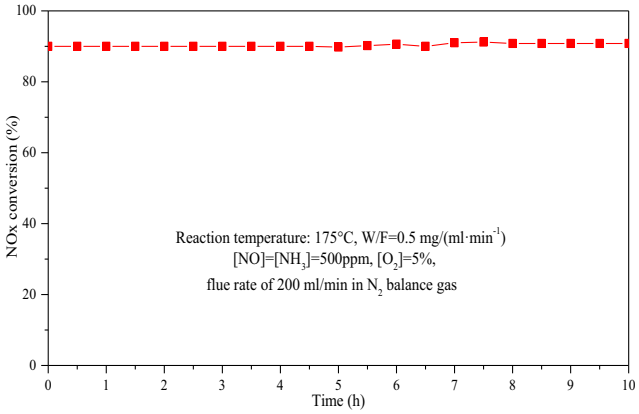

Fig. 13 Stability test of the $Fe_{(1)}$-$Ce_{(3)}$-$MnO_{x(7)}$/ACF_N catalyst

exhibited that Fe-doped $Ce_{(3)}$-$MnO_{x(7)}$/ACF_N could promote the dispersion of active components, improve the redox performance, and increase the acid amount. Meanwhile, the 15 wt% $Fe_{(1)}$-$Ce_{(3)}$-$MnO_{x(7)}$/ACF_N catalyst showed good water resistance and stability at 175 °C. This research is of great significance to the application of activated carbon fibers in the field of industrial denitrification, especially the denitrification of gas-fired boilers.

Funding information This study was funded by the National Key R&D Program of China (2017YFC0210303-01), the National Natural Science Foundation of China (21806009), the project funded by the China Postdoctoral Science Foundation (2018M631344), the Fundamental Research Funds for the Central Universities (FRF-TP-18-019A1), and the program "Promoting the Cooperative Innovation Among Beijing, Tianjin, and Hebei" (Z161100002716025).

References

Anthonysamy SBI, Binti AS, Mehrnoush K, Mohamed ARB (2018) A review of carbon-based and non-carbon-based catalyst supports for the selective catalytic reduction of nitric oxide. Beilstein J. Nanotechnol 9:740–761. https://doi.org/10.3762/bjnano.9.68

Cao F, Xiang J, Su S, Wang PY, Sun LS, Hu S, Lei SY (2014) The activity and characterization of MnOx-CeO_2-ZrO_2/γ-Al_2O_3 catalysts for low temperature selective catalytic reduction of NO with NH_3. Chem Eng J 243:347–354. https://doi.org/10.1016/j.apcatb.2013.10.049

Cao F, Su S, Xiang J, Wang PX, Hu S, Sun LS, Zhang AC (2015) The activity and mechanism study of Fe-Mn-Ce/γ-Al_2O_3 catalyst for low temperature selective catalytic reduction of NO with NH_3. Fuel 139:232–239. https://doi.org/10.1016/j.fuel.2014.08.060

Chang HZ, Li JH, Chen XY, Ma L, Yang SJ, Schwank JW, Hao JM (2012) Effect of Sn on MnOx-CeO_2 catalyst for SCR of NOx by ammonia: enhancement of activity and remarkable resistance to SO_2. Catal Commun 27:54–57. https://doi.org/10.1016/j.catcom.2012.06.022

Chen QL, Guo RT, Wang QS, Pan WG, Wang WH, Yang NZ, Lu CZ, Wang SX (2016) The catalytic performance of Mn/TiWOx catalyst for selective catalytic reduction of NOx with NH_3. Fuel 181:852–858. https://doi.org/10.1016/j.fuel.2016.05.045

Fan XY, Yang HS, Tian W, Nie AM, Hou TF, Qiu FM, Zhang XB (2011) Catalytic oxidation of chlorobenzene over MnOx/Al_2O_3-carbon nanotubes composites. Catal Letter 141(1):158–162. https://doi.org/10.1007/s10562-010-0450-9

Fan ZY, Shi JW, Gao C, Gao G, Wang BR, Wang Y, He C, Niu CM (2018) Gd-modified MnOx for the selective catalytic reduction of NO by NH_3: the promoting effect of Gd on the catalytic performance and sulfur resistance. Chem Eng J 348:820–830. https://doi.org/10.1016/j.cej.2018.05.038

Fang NJ, Guo JX, Shu S, Luo HD, Chu YH, Li JJ (2017) Enhancement of low-temperature activity and sulfur resistance of $Fe_{0.3}Mn_{0.5}Zr_{0.2}$ catalyst for NO removal by NH_3-SCR. Chem Eng J 325:114–123. https://doi.org/10.1021/am5038164

France LJ, Yang Q, Li W, Chen ZH, Guang JY, Guo DW, Wang LF, Li XH (2017) Ceria modified FeMnOx-enhanced performance and sulphur resistance for low-temperature SCR of NOx. Appl Catal B Environ 206:203–215. https://doi.org/10.1016/j.apcatb.2017.01.019

Gao FY, Tang XL, Yi HH, Li JY, Zhao SZ, Wang JG, Chu C, Li CL (2017a) Promotional mechanisms of activity and SO_2 tolerance of Co- or Ni-doped MnOx-CeO_2 catalysts for SCR of NOx with NH_3 at low temperature. Chem Eng J 317:20–31. https://doi.org/10.1016/j.cej.2017.02.042

Gao FY, Tang XL, Yi HH, Zhao SZ, Li CL, Li JY, Shi YR, Meng XM (2017b) A review on selective catalytic reduction of NOx by NH_3 over Mn-based catalysts at low temperatures: catalysts, mechanisms, kinetics and DFT calculations. Catalysts 7(7):199. https://doi.org/10.3390/catal7070199

Gao FY, Tang XL, Yi HH, Zhao SZ, Wang JG, Gu T (2019) Improvement of activity, selectivity and H_2O&SO_2-tolerance of micro-mesoporous $CrMn_2O_4$ spinel catalyst for low-temperature NH_3-SCR of NOx. Appl Surf Sci 466:411–424. https://doi.org/10.1016/j.apsusc.2018.09.227

Grzybek T, Klinik J, Motak M, Papp H (2008) Nitrogen-promoted active carbons as catalytic supports. Catal Today 137(2-4):235–241. https://doi.org/10.1016/j.cattod.2007.11.006

Hu G, Yang J, Tian YM, Kong BW, Liu QC, Ren S, Li JL, Kong M (2018) Effect of Ce doping on the resistance of Na over V_2O_5-WO_3/TiO_2 SCR catalysts. Mater Res Bull 104:112–118. https://doi.org/10.1016/j.materresbull.2018.04.009

Huang HC, Ye DQ, Huang BC, Wei ZL (2008) Vanadium supported on viscose-based activated carbon fibers modified by oxygen plasma for the SCR of NO. Catal Today 139(1-2):100–108. https://doi.org/10.1016/j.cattod.2008.08.028

Jiang LJ, Liu QC, Zhao Q, Ren S, Kong M, Yao L, Meng F (2018) Promotional effect of Ce on the SCR of NO with NH_3 at low temperature over MnOx supported by nitric acid-modified activated carbon. Res Chem Intermed 44(3):1729–1744. https://doi.org/10.1007/s11164-017-3194-y

Li P, Lu P, Zhai Y, Li C, Chen T, Qing R, Zhang W (2015a) Low temperature SCR of NO with catalysts prepared by modified ACF loading Mn and Ce: effects of modification method. Environ Technol 36(18):2390–2400. https://doi.org/10.1080/09593330.2015.1031829

Li J, Yang CW, Zhang QQ, Li Z, Huang W (2015b) Effects of Fe addition on the structure and catalytic performance of mesoporous Mn/Al-SBA-15 catalysts for the reduction of NO with ammonia. Catal Commun 62:24–28. https://doi.org/10.1016/j.catcom.2015.01.003

Li YL, Han XJ, Hou YQ, Guo YP, Liu YJ, Cui Y, Huang ZG (2018a) Role of CTAB in the improved H_2O resistance for selective catalytic reduction of NO with NH_3 over iron titanium catalyst. Chem Eng J 347:313–321. https://doi.org/10.1016/j.cej.2018.04.107

Li G, Wang BD, Wang ZC, Li ZH, Sun Q, Xu WQ, Li YL (2018b) Reaction mechanism of low-temperature selective catalytic reduction of NOx over Fe-Mn oxides supported on fly-ash-derived SBA-15 molecular sieves: structure-activity relationships and in situ DRIFT analysis. J Phys Chem C 122(35):20210–20231. https://doi.org/10.1021/acs.jpcc.8b03135

Liu ZM, Yi Y, Zhang SX, Zhu TL, Zhu JZ, Wang JG (2013) Selective catalytic reduction of NOx with NH_3 over Mn-Ce mixed oxide catalyst at low temperatures. Catal Today 216:76–81. https://doi.org/10.1016/j.cattod.2013.06.009

Liu ZM, Zhu JZ, Li JH, Ma L, Woo SI (2014) Novel Mn-Ce-Ti mixed-oxide catalyst for the selective catalytic reduction of NOx with NH_3. Acs Appl Mater Inter 6:14500–14508. https://doi.org/10.1021/am5038164

Liu ZM, Feng X, Zhou ZZ, Feng YJ, Li JH (2018a) Ce-Sn binary oxide catalyst for the selective catalytic reduction of NOx by NH_3. Appl Surf Sci 428:526–533. https://doi.org/10.1016/j.apsusc.2017.09.175

Liu ZM, Liu HY, Feng X, Ma LL, Cao XZ, Wang BY (2018b) Ni-Ce-Ti as a superior catalyst for the selective catalytic reduction of NOx with NH_3. Mol Catal 445:179–186. https://doi.org/10.1016/j.mcat.2017.11.028

Lu P, Li CT, Zeng GM, He LJ, Peng DL, Cui HF, Li SH, Zhai YB (2010) Low temperature selective catalytic reduction of NO by activated carbon fiber loading lanthanum oxide and ceria. Appl Catal B-Environ 96:157–161. https://doi.org/10.1016/j.apcatb.2010.02.014

Lu XL, Zou HQ, Zhang YB, Qiu HF, Zheng YY (2015) Low-temperature selective catalytic reduction of NO over carbon nanotubes supported MnO_2 fabricated by co-precipitation method. Micro Nano Lett 10(11):666–669. https://doi.org/10.1515/pac-2014-1117

Lu P, Xing Y, Li CT, Qing RP, Su W, Liu NA (2016) A reusable material with high performance for removing NO at room temperature: performance, mechanism and kinetics. Catal Sci Technol 6(10):3520–3528. https://doi.org/10.1039/c5cy01562f

Lu P, Li R, Xing Y, Li YR, Zhu TY, Yue HF, Wu WR (2018) Low temperature selective catalytic reduction of NOx with NH_3 by activated coke loaded with FexCoyCezOm: the enhanced activity, mechanism and kinetics. Fuel 233:88–199. https://doi.org/10.1016/j.cej.2017.02.148

Ma L, Seo CY, Nahata M, Chen XY, Li JH, Schwank JW (2018) Shape dependence and sulfate promotion of CeO_2 for selective catalytic reduction of NOx with NH_3. Appl Catal B Environ 232:246–259. https://doi.org/10.1016/j.apcatb.2018.03.065

Marani D, Silva RH, Dankeaw A, Norrman K, Werchmeister RML, Ippolito D, Gudik-Sørensen M, Hansen KK, Esposito V (2017) NOx selective catalytic reduction (SCR) on self-supported V-W-doped TiO_2 nanofibers. New J Chem 41(9):3466–3472. https://doi.org/10.1039/C6NJ03205B

Marbán G, Antu AR, Fuertes AB (2003) Low-temperature SCR of NOx with NH_3 over activated carbon fiber composite-supported metal oxides. Appl Catal B Environ 41(3):323–338. https://doi.org/10.1016/S0926-3373(02)00170-4

Meng DM, Xu Q, Jiao YL, Guo Y, Guo Y, Wang L, Lu GZ, Zhan WC (2018) Spinel structured $Co_aMn_bO_x$ mixed oxide catalyst for the selective catalytic reduction of NOx with NH_3. Appl Catal B Environ 221:652–663. https://doi.org/10.1016/j.apcatb.2017.09.034

Ramesh K, Chen LW, Chen FX, Liu Y, Wang Z, Han YF (2008) Re-investigating the CO oxidation mechanism over unsupported MnO, Mn_2O_3 and MnO_2 catalysts. Catal Today 131(1-4):477–482. https://doi.org/10.1016/j.cattod.2007.10.061

Shen BX, Liu T, Shi ZL, Shi JW, Yang TT, Zhao N (2008) Low-temperature selective catalytic reduction of NO with NH_3 based on MnOx-CeOx/ACFN. Front Chem Eng China 2(3):325–329. https://doi.org/10.1007/s11705-008-0053-9

Shen Q, Zhang LY, Sun NN, Wang H, Zhong LS, He C, Wei W, Sun YH (2017) Hollow MnOx-CeO_2 mixed oxides as highly efficient catalysts in NO oxidation. Chem Eng J 322:46–55. https://doi.org/10.1016/j.cej.2017.02.148

Shen BX, Zhu SW, Zhang X, Chi GL, Patel D, Si M, Wu CF (2018) Simultaneous removal of NO and Hg^0 using Fe and Co co-doped Mn-Ce/TiO_2 catalysts. Fuel 224:241–249. https://doi.org/10.1016/j.fuel.2018.03.080

Sun X, Guo RT, Liu SW, Liu J, Pan WG, Shi X, Qin H, Wang ZY, Qiu ZZ, Liu XY (2018a) The promoted performance of CeO_2 catalyst for NH_3-SCR reaction by NH_3 treatment. Appl Surf Sci 462:187–193. https://doi.org/10.1016/j.apsusc.2018.08.114

Sun P, Huang SX, Guo RT, Li MY, Liu SM, Pan WG, Fu ZG, Liu SW, Sun X, Liu J (2018b) The enhanced SCR performance and SO_2 resistance of Mn/TiO_2 catalyst by the modification with Nb: a mechanistic study. Appl Surf Sci 447:479–488. https://doi.org/10.1016/j.apsusc.2018.03.245

Sun CZ, Liu H, Chen W, Chen DZ, Yu SH, Liu AN, Dong L, Feng S (2018c) Insights into the Sm/Zr co-doping effects on N_2 selectivity and SO_2 resistance of a MnOx-TiO_2 catalyst for the NH_3-SCR reaction. Chem Eng J 347:27–40. https://doi.org/10.1016/j.cej.2018.04.029

Tang AD, Hu LQ, Yang XH, Jia YR, Zhang Y (2016) Promoting effect of the addition of Ce and Fe on manganese oxide catalyst for 1,2-dichlorobenzene catalytic combustion. Catal Commun 82:41–45. https://doi.org/10.1016/j.catcom.2016.04.015

Tang XL, Li CL, Yi HH, Wang LF, Yu QJ, Gao FY, Cui XX, Chu C, Li JY, Zhang RC (2018) Facile and fast synthesis of novel Mn_2CoO_4@rGO catalysts for the NH_3-SCR of NOx at low temperature. Chem Eng J 333:467–476. https://doi.org/10.1016/j.cej.2017.09.179

Thommes M, Kaneko K, Neimark AV, Olivier JP, Rodriguez-Reinoso F, Rouquerol J, Sing KS (2015) (2015) Physisorption of gases, with special reference to the evaluation of surface area and pore size distribution (IUPAC technical report). Pure Appl. Chem. 87(9-10):1051–1069. https://doi.org/10.1515/pac-2014-1117

Tian W, Yang HS, Fan XY, Zhang XB (2011) Catalytic reduction of NOx with NH_3 over different-shaped MnO_2 at low temperature. J Hazard Mater 188(1-3):105–109. https://doi.org/10.1016/j.jhazmat.2011.01.078

Wan YP, Zhao WR, Tang Y, Li L, Wang HJ, Cui YL, Gu JL, Li YS, Shi JL (2014) Ni-Mn bi-metal oxide catalysts for the low temperature SCR removal of NO with NH_3. Appl Catal B Environ 148-149:114–122. https://doi.org/10.1016/j.apcatb.2013.10.049

Wang YL, Ge CZ, Zhan L, Li C, Qiao WM, Ling LC (2012) MnOx-CeO_2/activated carbon honeycomb catalyst for selective catalytic reduction of NO with NH_3 at low temperatures. Ind Eng Chem Res 51(36):11667–11673. https://doi.org/10.1021/ie300555f

Wang MX, Liu HN, Huang ZH, Kang FY (2014) Activated carbon fibers loaded with MnO_2 for removing NO at room temperature. Chem Eng J 256:101–106. https://doi.org/10.1016/j.cej.2014.06.108

Wang WT, Herreros JM, Tsolakis A, York APE (2015) Increased NO_2 concentration in the diesel engine exhaust for improved Ag/Al_2O_3 catalyst NH_3-SCR activity. Chem Eng J 270:582–589. https://doi.org/10.1016/j.cej.2015.02.067

Wang DH, Yao Q, Hui SE, Niu YQ (2018) N_2O and NO formation from NH_3 oxidation over MnO_2/TiO_2 catalysts. Fuel 234:650–655. https://doi.org/10.1016/j.fuel.2018.07.073

Wu ZB, Jiang B, Liu YQ, Wang HQ, Jin RB (2007) DRIFT study of manganese/titania-based catalysts for low-temperature selective catalytic reduction of NO with NH_3. Environ Sci Technol 41:5812–5817. https://doi.org/10.1021/es0700350

Xu Q, Su RJ, Cao L, Li YQ, Yang CY, Luo Y, Street J, Jiao PC, Cai LL (2017) Facile preparation of high-performance Fe-doped Ce-Mn/TiO_2 catalysts for the low-temperature selective catalytic reduction of NOx with NH_3. RSC Adv. 7(77):48785–48792. https://doi.org/10.1039/C7RA07854D

Yan QH, Chen SN, Zhang C, O'Hare D, Wang Q (2018) Synthesis of $Cu_{0.5}Mg_{1.5}Mn_{0.5}Al_{0.5}Ox$ mixed oxide from layered double hydroxide precursor as highly efficient catalyst for low-temperature selective catalytic reduction of NOx with NH_3. J Colloid Interface Sci 526:63–74. https://doi.org/10.1016/j.jcis.2018.04.099

You XC, Sheng ZY, Yu DQ, Yang L, Xiao XX, Wang SS (2017) Influence of Mn/Ce ratio on the physicochemical properties and

catalytic performance of graphene supported MnOx-CeO_2 oxides for NH_3-SCR at low temperature. Appl Surf Sci 423:845–854. https://doi.org/10.1016/j.apsusc.2017.06.226

Yu CL, Huang BC, Dong LF, Chen F, Liu XQ (2017) In situ FT-IR study of highly dispersed MnOx/SAPO-34 catalyst for low-temperature selective catalytic reduction of NOx by NH_3. Catal Today 281: 610–620. https://doi.org/10.1016/j.cattod.2016.06.025

Zhang L, Zhang DS, Zhang JP, Cai SX, Fang C, Huang L, Li HR, Gao RH, Shi LY (2013) Design of meso-TiO_2@MnOx-CeOx/CNTs with a core-shell structure as DeNOx catalysts: promotion of activity, stability and SO_2-tolerance. Nanoscale 5(20):9821–9829. https://doi.org/10.1039/c3nr03150k

Zhang SG, Zhang BL, Liu B, Sun SL (2017) A review of Mn-containing oxide catalysts for low temperature selective catalytic reduction of NOx with NH_3: reaction mechanism and catalyst deactivation. RSC Adv 7(42):26226–26242. https://doi.org/10.1039/c7ra03387g

Zhang SB, Zhao YC, Yang JP, Zhang JY, Zheng CG (2018) Fe-modified MnOx/TiO_2 as the SCR catalyst for simultaneous removal of NO and mercury from coal combustion flue gas. Chem Eng J 348:618–629. https://doi.org/10.1016/j.cej.2018.05.037

Zhou LL, Li CT, Zhao LK, Zeng GM, Gao L, Wang Y, Yu ME (2016) The poisoning effect of PbO on Mn-Ce/TiO_2 catalyst for selective catalytic reduction of NO with NH_3 at low temperature. Appl Surf Sci 389:532–539. https://doi.org/10.1016/j.apsusc.2016.07.136

Zhu LL, Huang BC, Wang WH, Wei ZL, Ye DQ (2011) Low-temperature SCR of NO with NH_3 over CeO_2 supported on modified activated carbon fibers. Catal Commun 12(6):394–398. https://doi.org/10.1016/j.catcom.2010.10.028

Zuo SF, Huang QQ, Li J, Zhou RX (2009) Promoting effect of Ce added to metal oxide supported on Al pillared clays for deep benzene oxidation. Appl Catal B-Environ 91(1-2):204–209. https://doi.org/10.1016/j.apcatb.2009.05.025